CONSTRUCTION AND EXPERIMENTAL STUDY OF AN INTERMITTENT DRYING MODEL FOR PADDY BASED ON GLASS TRANSITION

/

基于玻璃化转变的稻谷间歇干燥模型的构建及试验研究

Chengjiang TANG[1)], Guangyu MA*[1)]
Department of Mechanical and Electrical Engineering, Heilongjiang Agricultural Vocational and Technical College, Jiamusi / P. R. China
Tel: 13845410577; E-mail: hnzytcj@163.com
Corresponding author: Guangyu Ma
DOI: https://doi.org/10.35633/inmateh-77-126

Keywords: *paddy, glass transition, intermittent drying, model, experiment*

ABSTRACT

This study addresses the quality deterioration induced by starch phase transitions during rice drying, which arise from coupled temperature and moisture variations. A mathematical model for intermittent drying is proposed that integrates the glass transition mechanism with a three-dimensional, realistic grain geometric structure. The model was validated using continuous drying (CD) and two-stage intermittent drying (2SID) experiments. The results showed excellent agreement between simulations and experimental data, with correlation coefficients exceeding 0.95. Model analysis revealed that during 2SID at 45 °C, the glassy region rapidly formed from the grain surface inward, accounting for approximately 19.6% of the total grain volume at the end of the first drying stage. After a 20-min tempering period, the internal moisture gradient was effectively reduced, and the glassy region expanded only slightly by about 2.1%. Following the second drying stage, the glassy region increased to approximately 47.9%, while the central layer of the grain remained in the rubbery state throughout the process. Compared with CD, 2SID not only reduced the total drying time by approximately 9.09% but, more importantly, significantly regulated the internal moisture distribution through the tempering stage, thereby helping to mitigate fissure formation and improve head rice yield. The proposed model provides a reliable theoretical framework and predictive tool for optimizing intermittent drying parameters and simultaneously enhancing drying efficiency and paddy rice processing quality.

摘要

本研究针对稻谷干燥过程中因温度与水分变化导致的淀粉相态转变及其引发的品质劣化问题，提出了一种融合玻璃化转变机制与三维真实籽粒几何结构的间歇干燥数学模型。模型通过连续干燥（CD）和两段间歇干燥（2SID）实验进行验证，结果表明模拟数据与试验结果高度吻合，相关系数均超过0.95。模型分析显示，在45°C的2SID过程中，玻璃化区域首先从表层快速形成，第一干燥阶段结束时约占籽粒体积的19.6%；经20分钟缓苏，水分梯度有效降低，玻璃区仅小幅扩展约2.1%；第二干燥阶段后，玻璃区总面积增至约47.9%，而中心层始终维持在橡胶态。与CD相比，2SID不仅将总干燥时间缩短约9.09%，更重要的是通过缓苏阶段显著调控了内部水分分布，从而有助于减少裂纹产生、提升整精米率。该模型为优化间歇干燥工艺参数、协同提升干燥效率与稻谷加工品质提供了可靠的理论工具与预测手段。

INTRODUCTION

Freshly harvested paddy rice typically has a high moisture content. If the moisture level is not promptly reduced to a safe threshold, quality deterioration and microbial spoilage are likely to occur during storage. Therefore, drying is a critical operation to ensure the safe storage and stable processing performance of paddy (*Wang et al., 2024*). During the drying process, the internal temperature field and moisture distribution within the grain evolve simultaneously, resulting in non-uniform shrinkage and coupled heat–moisture transfer effects across different regions of the kernel. These processes induce the formation and accumulation of differential internal stresses, which may manifest as crack initiation and propagation during subsequent milling operations, ultimately leading to kernel breakage and a reduction in head rice yield (*Nasrnia et al., 2024*).

[1] *Chengjiang Tang, master degree*; *Guangyu Ma, master degree.*

Under continuous drying conditions, inappropriate process parameters may not only deteriorate rice quality but also cause thermal damage and structural degradation of the grains (*Liu et al., 2023*). In contrast, intermittent drying introduces a tempering stage between drying periods, allowing moisture redistribution within the grain (*Guo et al., 2024*). During tempering, moisture migrates from the central region toward the near-surface layers, thereby alleviating internal moisture gradients and thermo-hygrometric non-uniformity (*Liu et al., 2024*). Based on this mechanism, multi-stage intermittent drying has been shown to significantly improve final product quality and processing suitability. In this drying mode, moisture removal is not completed in a single step but proceeds sequentially following a "drying–tempering–redrying" scheme. During the tempering stage, moisture exchange between the grain and the surrounding air is typically minimized, such that internal moisture migration and equilibration dominate, thereby establishing more stable initial conditions for the subsequent drying stage (*Mahmood et al., 2024*).

Starch is the primary constituent of paddy rice and is essentially a high-molecular-weight polymer composed of glucose monomers. The thermal response of starch varies markedly with moisture content and temperature, enabling transitions between two physical states, namely the glassy and rubbery states, which are closely associated with drying conditions (*Wang et al., 2023*). In the rubbery state, molecular mobility is enhanced, and moisture diffusivity is generally higher than in the glassy state, thereby facilitating more rapid dehydration. Conversely, when the grain surface is subjected to intense drying, surface moisture is removed rapidly, causing the outer layers to enter the glassy state earlier than the interior (*Wang et al., 2022*). Given these characteristics, the rational determination of intermittent drying parameters requires distinguishing and analyzing the drying behavior of different grain regions at various stages of the process (*Liu et al., 2023*). Moreover, crack initiation and propagation are often closely related to the timing and evolution of the glass transition. Consequently, understanding the temporal progression and spatial distribution of glass transition during drying is essential for elucidating the underlying mechanisms of fissure formation (*Baidhe & Clementson, 2024*). In recent years, numerical simulation techniques have increasingly become an important tool for investigating heat and mass transfer mechanisms and process optimization in agricultural seed drying (*Delele et al., 2023*). By developing mathematical models or employing computational fluid dynamics (CFD) approaches, the temperature field, moisture distribution, and transport pathways within seeds and the surrounding airflow during drying can be quantitatively characterized, thereby compensating for the limitations of experimental methods in spatial resolution and temporal continuity. Previous studies have demonstrated that numerical simulation based analyses can effectively elucidate the effects of drying parameters on seed drying kinetics and quality evolution, providing a solid theoretical basis for the design of drying equipment and the optimization of operating conditions (*Cârlescu et al., 2018; Arsenoaia et al., 2019*).

Although various models have been developed to describe the intermittent drying behavior of paddy rice, studies that explicitly incorporate glass transition theory into such models remain limited. In addition, many existing drying models adopt idealized geometric representations of rice kernels, often approximating them as spheres or ellipsoids. Such simplifications deviate from the actual grain morphology and may introduce significant errors in the prediction of heat and mass transfer pathways, surface area distribution, and local gradients, thereby compromising the reliability of model outputs. In light of these limitations, the present study develops a mathematical model for intermittent drying of paddy rice based on a realistic three-dimensional grain geometry and explicitly incorporates the concept of glass transition to characterize state evolution. The proposed model provides a theoretical basis for identifying and optimizing key process parameters in intermittent drying, with the aim of simultaneously improving drying efficiency and final product quality.

MATERIALS AND METHODS

Sample preparation

The experimental material used in this study was the japonica rice cultivar Longjing 31, developed by the Jiamusi Rice Research Institute, Heilongjiang Academy of Agricultural Sciences, China. To ensure sample uniformity and experimental reproducibility, impurities such as stones, straw, and dust were removed prior to experimentation. The initial moisture content of the paddy rice samples was 27% on a dry basis. Before the drying experiments, the samples were sealed in polyethylene bags and stored in a refrigerator at 4 °C to maintain moisture stability. Prior to each drying run, the sealed samples were removed from cold storage and equilibrated under laboratory conditions for approximately 4 h to allow thermal and moisture redistribution at ambient temperature. This procedure minimized the influence of initial temperature differences on the drying process (*Ying & Spang, 2024*).

Experimental procedure

To obtain the key parameters required for model development and to calibrate and validate the proposed model, a series of drying experiments were conducted under various operating conditions. A schematic diagram of the hot-air drying system used in this study is shown in Fig. 1. The system was equipped with integrated modules for real-time monitoring of sample mass, relative humidity, energy consumption, and temperature, enabling continuous acquisition of process data. All experiments were performed at a constant air velocity of 0.5 $m \cdot s^{-1}$. To support numerical simulation and model validation, both continuous drying (CD) and two-stage intermittent drying (2SID) experiments were carried out at a drying temperature of 45 °C. For the 2SID process, the first drying stage was conducted for 40 min, after which the samples were immediately transferred into sealed plastic bags and placed in a vacuum drying oven maintained at 45 °C for a 20 min tempering period. Subsequently, the tempered samples were returned to the drying chamber for the second drying stage. The selection of the tempering time was based on preliminary experimental results. When the tempering time was shorter than 20 min, moisture redistribution within the grains was insufficient, whereas further extension of the tempering period provided only limited improvement in moisture gradient relaxation and drying kinetics while markedly increasing the overall processing time. Therefore, a tempering time of 20 min was selected in this study by considering both moisture equilibration efficiency and process efficiency. The drying process was terminated when the moisture content of the samples reached 17% on a dry basis. After each experimental run, the total drying time as well as the moisture content (MC) evolution and its kinetic characteristics were measured and recorded for model calibration and performance evaluation.

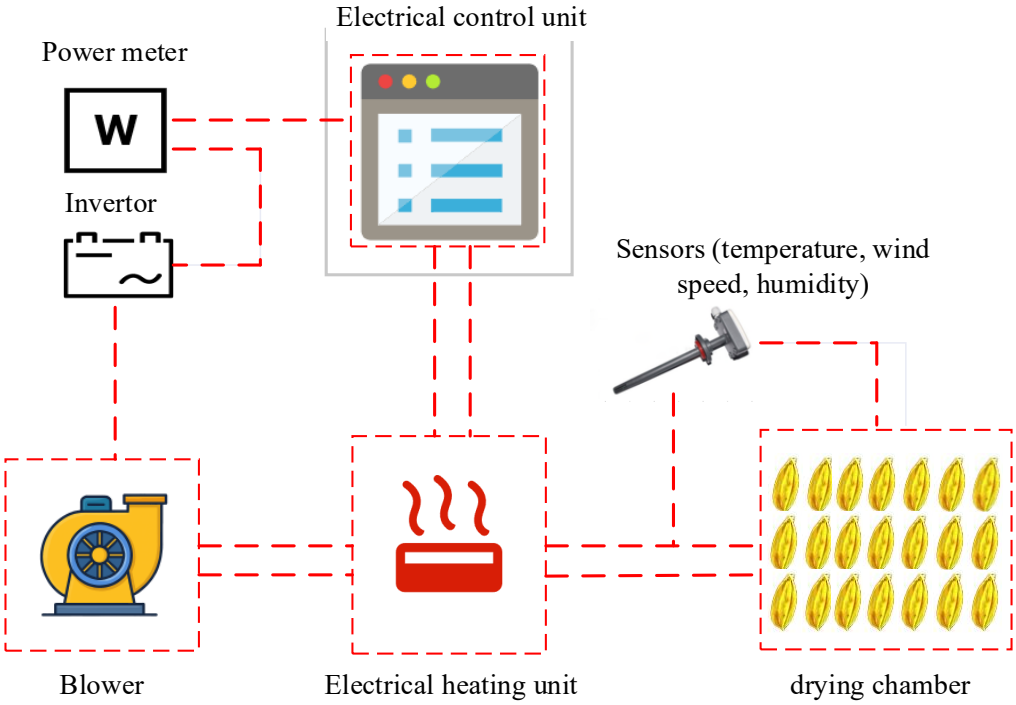

Fig. 1 - Schematic diagram of the hot-air drying system

Development of the mathematical model

A mathematical model was developed in this study to describe the multi-stage intermittent drying process of paddy. The corresponding governing equations, as well as the associated initial and boundary conditions, are systematically presented. The model is formulated at the macroscopic scale with the following assumptions: moisture within the grain exists only in the liquid phase; moisture first migrates from the interior of the grain to the surface and is subsequently removed via evaporation at the surface. To simplify computation, the effect of grain volume shrinkage on heat and mass transfer during drying is neglected (*Wang et al., 2024*). Previous studies suggest that under conventional hot-air drying and intermittent drying conditions, the volumetric shrinkage of rice grains is relatively small. As a result, its effect on the effective moisture diffusivity and the overall drying kinetics is generally limited and may be reasonably neglected in macroscopic models without leading to a significant reduction in predictive accuracy (*Zhao et al., 2019*). Moisture migration inside the grain is assumed to be governed solely by diffusion, and the paddy rice kernel is treated as an isotropic medium.

Heat and mass exchanges between the grain and the external drying medium are described using convective boundary conditions. In addition, the temperature field and moisture content (MC) distribution inside the grain are assumed to be uniform at the onset of drying (*Zhang et al., 2024*).

Internal energy transport within the paddy rice grain is governed by Fourier's law of heat conduction in conjunction with the principle of energy conservation, as expressed in Eq. (1):

$$\rho C_p \frac{\partial T}{\partial t} = \nabla (k \nabla T) + Q \tag{1}$$

where T is the grain temperature (°C); ρ is the density of paddy rice (kg·m^{-3}), determined by the liquid displacement method; C_p is the specific heat capacity (J·kg^{-1}·°C^{-1}); k is the effective thermal conductivity of the rice kernel (W·m^{-1}·°C^{-1}); and Q is the volumetric heat source term (W·m^{-3}). The volumetric heat source represents the equivalent energy consumption associated with moisture evaporation, as the latent heat required for surface evaporation is supplied by the grain itself.

The effective thermal conductivity k and volumetric heat source Q are calculated using Eqs. (2) and (3).

$$k = \frac{0.0637 + 0.0958M}{0.656 - 0.475M} \tag{2}$$

$$Q = \rho h_t \frac{\partial M}{\partial t} \tag{3}$$

where M is the moisture content on a dry basis (kg·kg^{-1}) and h_t is the latent heat of vaporization of water (J·kg^{-1}).

The initial condition for heat transfer is given in Eq. (4). Heat exchange between the grain and surrounding air is dominated by convection, and the heat flux is proportional to the temperature difference between the grain surface and the drying air. Accordingly, Eqs. (4)–(7) are used as thermal boundary conditions.

$$T\big|_{t=0} = T_0 \tag{4}$$

$$-n \cdot q = q_0 \tag{5}$$

$$-n \cdot (-k \nabla T) = H(T_{air} - T) \tag{6}$$

$$-k \cdot \left(\frac{\partial T}{\partial n}\right) = H(T - T_{air}) \tag{7}$$

where H is the convective heat transfer coefficient (W·m^{-2}·°C^{-1}), T_{air} is the drying air temperature (°C), and n is the outward normal vector at the grain surface.

Moisture migration within the paddy rice grain is described using Fick's second law of diffusion, as shown in Eq. (8).

$$\frac{\partial M}{\partial t} = \nabla (D_{eff} \nabla M) \tag{8}$$

where D_{eff} is the effective moisture diffusivity (m^2·s^{-1}).

The initial moisture distribution within the grain is defined by Eqs. (9) and (10).

$$M\big|_{t=0} = M_0 \tag{9}$$

$$\frac{\partial M}{\partial t}\big|_{t=0} = 0 \tag{10}$$

To ensure mass conservation, the amount of moisture evaporated at the surface equals the amount transported from the interior. Thus, Eq. (11) is applied as the mass transfer boundary condition.

$$-D_{eff} \frac{\partial M}{\partial n} = h_D (M - M_e) \tag{11}$$

where M_e is the equilibrium moisture content, and h_D is the convective mass transfer coefficient (m·s^{-1}).

The equilibrium moisture content and mass transfer coefficient are calculated using Eqs. (12) and (13).

$$M_e = \left(\frac{-\ln(1 - RH)}{0.00004127(T + 49.828)}\right)^{1/2.1191} \tag{12}$$

$$h_D = \frac{D_{eff}\left[2.0 + 0.552\,\mathrm{Re}^{1/2}\, Sc^{1/3}\right]}{R_{eq}} \tag{13}$$

where RH is the relative humidity of drying air (%), Re is the Reynolds number, R_{eq} is the equivalent radius of the rice kernel, and Sc is the Schmidt number.

The Reynolds and Schmidt numbers are calculated using Eqs. (14) and (15).

$$Sc = \frac{\mu_a}{\rho_a D_{eff}} \tag{14}$$

$$\mathrm{Re} = \frac{2\left(\rho_a R_{eq} U_a\right)}{\mu_a} \tag{15}$$

where μ_a is the dynamic viscosity of air (N·s·m^{-2}), ρ_a is the air density (kg·m^{-3}), U_a is the drying air velocity (m·s^{-1}).

To represent tempering conditions, the mass transfer boundary conditions were modified. Under tempering, the boundary constraints are described by Eqs. (16) and (17).

$$\frac{\partial M}{\partial n}\Big|_s = 0 \tag{16}$$

$$M\left(x, y, z, 0\right) = f\left(x, y, z, t_1\right) \tag{17}$$

Based on experimental moisture ratio (MR) data, the effective moisture diffusivity was estimated using an anti-logarithmic method, as shown in Eqs. (18) and (19). The effective moisture diffusivity was assumed to be constant within each drying stage and updated between stages to account for different drying regimes (*Le et al., 2019*).

$$MR = \frac{M - M_e}{M_0 - M_e} \tag{18}$$

$$D_{eff} = \frac{sr^2}{t} \tag{19}$$

where:

r is the equivalent radius of the paddy kernel (m), and s is the slope of the linear relationship between ln(MR) and drying time t. The calculated D_{eff} values at different temperatures are listed in Table 1.

Table 1

Effective moisture diffusivity at different hot-air drying temperatures

Drying temperature (°C)	Effective moisture diffusivity (m²·s⁻¹)
35	4.2×10^{-12}
45	8.6×10^{-12}
55	9.2×10^{-12}
65	1.2×10^{-11}

Based on these results, a generalized Arrhenius-type relationship was established using logarithmic regression, as expressed in Eq. (20) (*Srisang et al., 2015*).

$$D_{eff} = \left(7\times10^{-11}\right)\exp\left(\frac{-107.3}{T}\right) \tag{20}$$

Determination of glass transition temperature (T_g) and definition of the state function

In this study, the glass transition temperature (T_g) of paddy rice was determined at five moisture contents on a dry basis (28%, 23%, 20%, 18%, 17%, and 14% d.b.) using differential scanning calorimetry (DSC 3, Mettler Toledo, USA). After loading the sample into the instrument, liquid nitrogen was introduced to cool the specimen to −40°C, and the temperature was held for 10 min to achieve thermal equilibrium. The sample was then heated to 90°C at a rate of 10°C·min^{-1} and held for 10 min to stabilize the system. Subsequently, the sample was cooled to 40 °C at the same rate; after sufficient equilibration, a second heating run was performed to 90°C using the identical heating rate. Based on the above thermal analysis procedure, the results are shown in Fig. 2.

Because temperatures above the glass transition correspond to the rubbery state, a state variable S was introduced into the governing equations to facilitate discrimination of state domains within the modeling framework, as defined in Eq. (21). This variable is jointly determined by the instantaneous temperature of each computational element (T_i) and its corresponding T_g, and can be incorporated as a component of the model's dependent variables. A positive S indicates that the element is in the rubbery state, whereas a negative S corresponds to the glassy state (*Chayjan et al., 2024*).

$$S = T_i - T_g \tag{21}$$

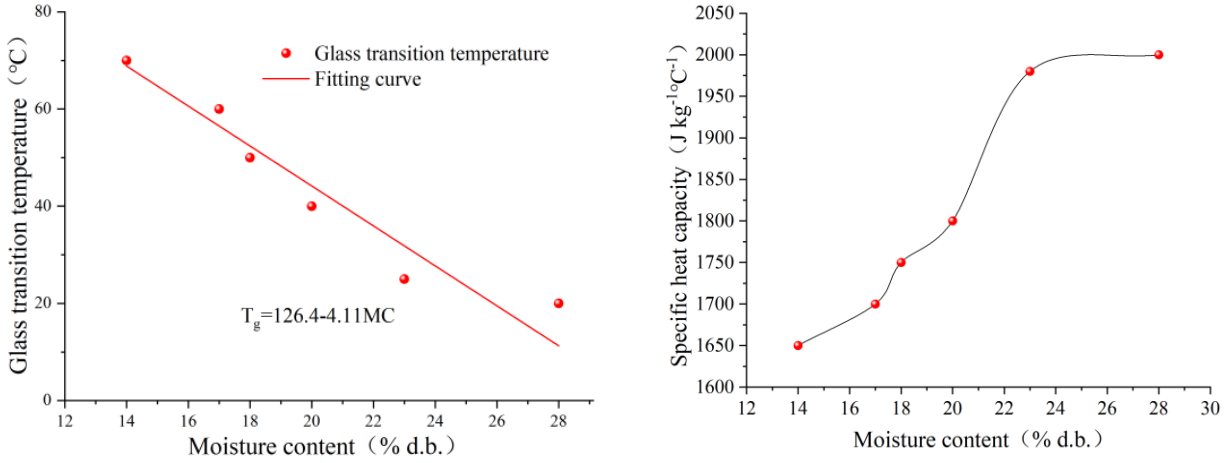

(a) Glass transition curve (b) Specific heat capacity variation curve

Fig. 2 - Relationships between specific heat capacity and glass transition temperature (T_g) of paddy rice and moisture content measured by DSC

Geometric model preparation and numerical solution

To obtain the realistic three-dimensional morphology of the kernels, a three-dimensional optical scanning workflow was employed to construct point-cloud data via multi-view, high-resolution optical imaging and point acquisition. A GOM ATOS system (ZEISS, Braunschweig, Germany) was used, providing a scanning accuracy of up to 1 μm. The resulting kernel point-cloud model was exported as a stereolithography (STL) file. The point cloud was then subjected to surface reconstruction, and the reconstructed surface was further converted into a solid geometric model (STP format). Accordingly, a true geometry that preserves kernel-level geometric details was established in a Cartesian coordinate system, providing a reliable geometric basis for subsequent model development and numerical computation. For numerical implementation, the finite element method was adopted to solve the developed nonlinear system of partial differential equations together with the associated boundary conditions, initial conditions, and thermophysical properties. The coupled heat–moisture transport equations were solved using COMSOL Multiphysics 5.3 (*Nasrnia et al., 2024*).

RESULTS AND DISCUSSIONS

Volume-averaged temperature kinetics and temperature distribution

When the 2SID protocol was implemented at a drying-air temperature of 45°C, the simulated temporal evolution of the volume-averaged temperature of paddy rice is shown in Fig. 3.

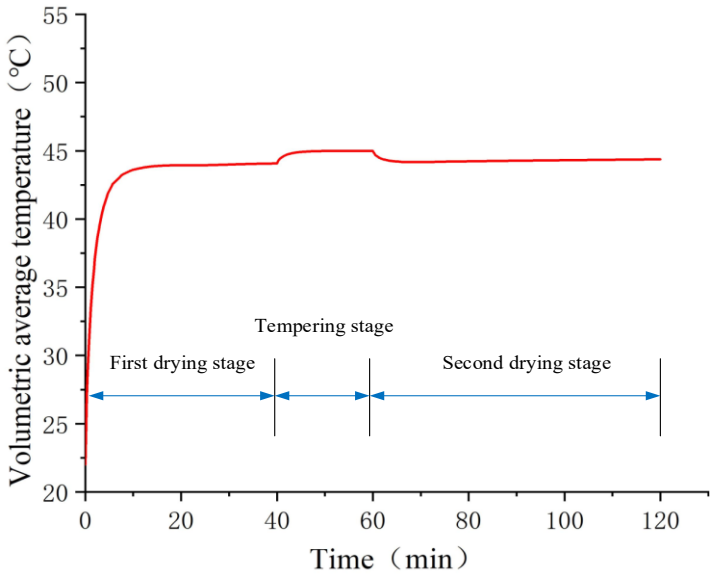

Fig. 3 - Simulated variation of the volume-averaged temperature of paddy rice with time as predicted by the proposed model

The results indicate that, shortly after the onset of the first drying stage, the mean grain temperature increased rapidly from the initial value (22°C) and gradually approached the temperature of the hot-air drying medium (45°C). This rapid heating behavior is closely associated with the small characteristic size of the kernels, which facilitates efficient heat conduction from the surface toward the interior and enables fast heat transfer to the central region. Because the tempering step was conducted under the same temperature condition as the drying step, the volume-averaged grain temperature remained essentially stable upon entering the tempering stage, with no pronounced fluctuations observed. During the second drying stage, the volume-averaged temperature was maintained at approximately 45 °C and remained nearly constant until the end of the drying process.

The simulated temperature fields at selected time points during the first drying stage, the tempering stage, and the second drying stage of the 2SID process are presented in Fig. 4. At the onset of the first drying stage, the temperature of all computational cells within the domain was uniform and equal to the ambient value (22°C). Once drying was initiated, heat was transferred from the surface toward the interior primarily via conduction, leading to a rapid attenuation of the initially developed temperature gradient. Accordingly, the simulation shows that the temperature gradient formed at the early heating period was markedly reduced and nearly disappeared within approximately 5 min. The kernel temperature became quickly homogenized, and by ~10 min the entire grain reached about 50°C, with negligible temperature differences within the interior. Upon entering the tempering stage, because the process was conducted under the same thermal condition as the preceding drying step, the temperature across different layers remained essentially constant at approximately 45°C. After tempering, the second drying stage was initiated at 60 min, and the system continued operating at 45°C; therefore, no pronounced changes in the temperature distribution were observed. Overall, during paddy rice drying, the temperatures across layers approached and reached the drying-air temperature within a short period, and the subsequent process proceeded in a quasi-isothermal manner until completion. In other words, appreciable temperature gradients were mainly confined to the brief initial heating period of the first drying stage.

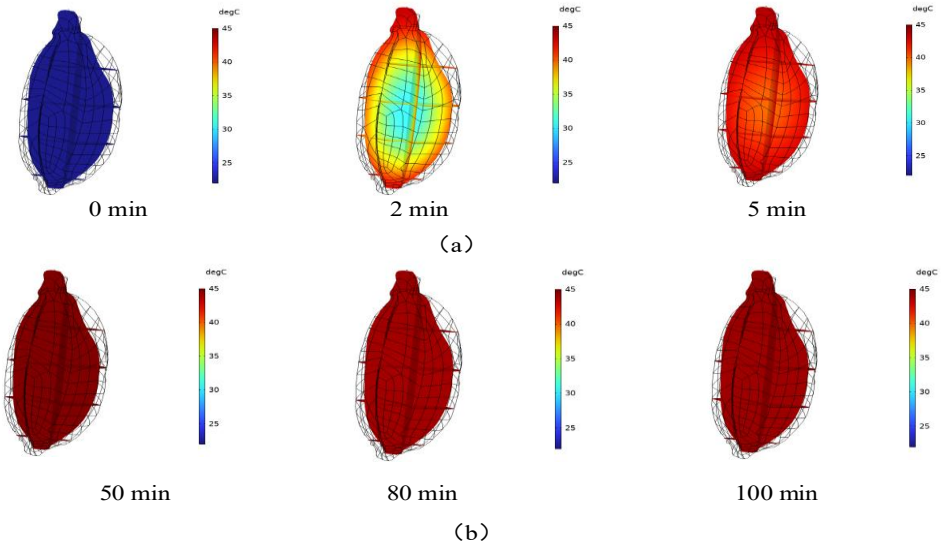

Fig. 4 -Temperature distribution inside paddy rice predicted by the developed model: (a) first drying stage; (b) tempering and second drying stage

Moisture content kinetics and moisture distribution of paddy

At 45°C, the kinetics of the volume-averaged moisture content of paddy rice during continuous drying (CD) and the two-stage intermittent drying process (2SID) are compared in Fig. 5, where experimental measurements are plotted against model predictions. To quantitatively evaluate the predictive performance of the model, the root mean square error (RMSE) and the correlation coefficient (R) between simulated and measured values for both drying modes under different air-temperature conditions are summarized in Table 2. These statistical indicators demonstrate that the developed model captures the moisture-content evolution with good agreement, thereby supporting the reliability of the simulation results in a statistical sense. In terms of drying duration, the predicted overall drying time for the 2SID process was approximately 100 min, whereas that for CD was about 110 min. Compared with CD, 2SID reduced the drying time by 9.09%.

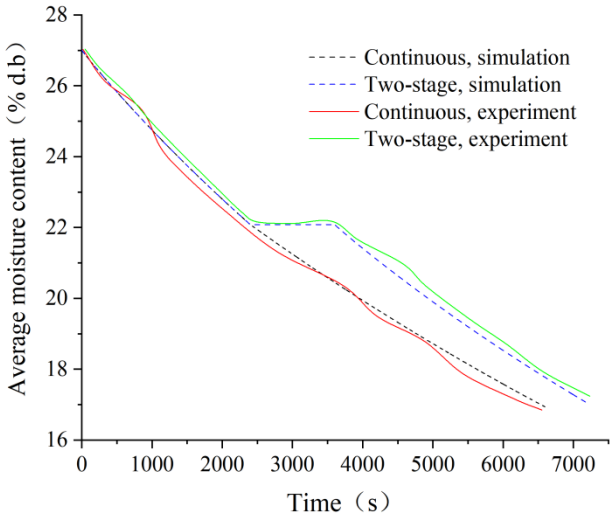

Fig. 5 - Comparison of experimental and simulated results for the temporal variation of the volume-averaged moisture content of paddy rice during CD and 2SID

An important objective of this study was to elucidate the spatial characteristics of the transient intra-kernel moisture content (MC) distribution of paddy rice during each stage of intermittent drying. Such information provides direct insight into the formation and evolution of internal moisture gradients, thereby offering a basis for selecting more appropriate drying strategies and reducing the risk of quality deterioration. Figure 6 illustrates the simulated transient MC distributions within the kernel during the 2SID process, including the first drying stage, tempering, and the second drying stage.

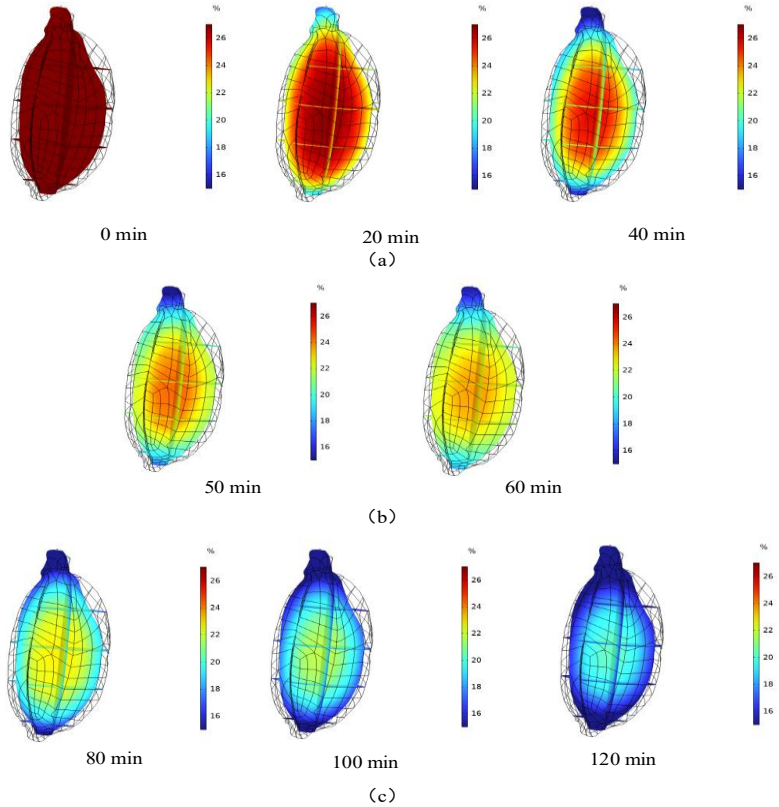

Fig. 6 - Predicted moisture content distribution within paddy rice kernels during two-stage intermittent drying at 45 °C: (a) first drying stage; (b) tempering stage; (c) second drying stage

As shown in Fig. 6(a), at the beginning of the first drying stage, the MC was relatively uniform across the kernel layers (approximately 27% d.b.). As drying proceeded, moisture continuously evaporated from the surface, whereas outward migration of internal moisture was progressively constrained. Consequently, a moisture gradient gradually developed between layers and intensified with time.

By the end of the first drying stage (40 min), pronounced MC differences had emerged within the kernel. Such moisture non-uniformity may induce incipient fissures and further develop into cracks. Therefore, sufficient time is required to allow moisture redistribution from the center toward the surface, so that subsequent moisture removal can occur more efficiently at the surface. Based on this consideration, heating was terminated at the end of the first drying stage and the process was switched to the tempering step. The spatiotemporal MC distribution during tempering is presented in Fig. 6(b). A large moisture gradient was still evident at the onset of tempering; however, the gradient was markedly reduced after approximately 20 min of tempering. This behavior can be attributed to the suppression of surface evaporation during tempering, such that moisture transport was dominated by internal redistribution. Moisture migrated from the center to the middle layers and subsequently toward the surface, thereby substantially reducing inter-layer differences. Tempering can effectively mitigate unfavorable differential stresses within the kernel, while also improving the conditions for the subsequent drying stage by facilitating the removal of surface moisture. Therefore, appropriate determination of tempering conditions is critical for both drying efficiency and quality preservation, and such optimization can be assisted by the model developed in this study.

Table 2

RMSE and correlation coefficient (R) for CD and 2SID at different drying-air temperatures

Drying-air temperature (°C)	CD		2SID	
	RMSE	R	RMSE	R
35	0.42	0.95	0.56	0.95
45	0.63	0.96	0.46	0.95
55	0.56	0.95	0.65	0.96
65	0.74	0.95	0.81	0.95

Figure 7 presents the simulated temporal variation of moisture content (MC) at three representative locations within the kernel—surface (A), middle layer (B), and center (C)—to compare the behaviors under continuous drying (CD) and two-stage intermittent drying (2SID). The MC evolutions differed among the locations, reflecting the formation and evolution of moisture gradients across layers. During the period of 0–50 min, the MC trends at points B and C were essentially similar for CD and 2SID, showing no pronounced differences. In contrast, at point A, a transient rebound was observed under 2SID during 40–50 min (tempering), where the MC increased to a peak of 21.9%, approximately 1% higher than the corresponding value under CD, and then gradually decreased. Under CD, however, the MC at point A decreased continuously throughout the process. After the onset of the second drying stage, moisture at the surface (point A) again migrated outward and was removed to the surroundings. At t = 100 min, the moisture reduction at point B was 22.2% and 22.8% for CD and 2SID, respectively; at point C, the corresponding values were 17.4% and 18.1%; and at point A, 34.4% and 32.6%, respectively. Overall, the moisture gradient between A and B was markedly larger than that between B and C. Under CD, the A–B gradient increased more rapidly. Under 2SID, this gradient reached a relatively high level at the end of the first drying stage (40 min) and then decreased progressively once tempering started. As discussed above, the second drying stage further alleviated the inter-layer moisture differences. Therefore, compared with CD, 2SID effectively reduced the residual moisture gradient at the late drying stage, which is beneficial for lowering the risk of fissure and crack formation in paddy rice. Overall, compared with continuous drying (CD), two-stage intermittent drying (2SID) significantly improves the internal moisture gradient distribution of rice grains while maintaining drying efficiency. Quantitative results indicate that at 45 °C, the 2SID process shortens the total drying time by approximately 9.09% and effectively reduces the residual moisture gradient between the surface and intermediate layers at the final stage of drying. The tempering stage promotes moisture redistribution from the center toward the outer layers, thereby suppressing the continuous accumulation of moisture gradients and achieving a synergistic optimization between drying efficiency enhancement and moisture gradient alleviation.

Kinetics of state transition (from rubbery to glassy)

To characterize the state transition of kernels during each stage of 2SID using the developed model, a longitudinal cross-section of a rice kernel was considered along the major axis. The temperature, MC, and state function (S) were extracted for elements at different times and evaluated against the glass transition line. The instantaneous state of each element was then determined.

In Fig. 8, the green region represents the rubbery state, whereas the dark-blue region indicates the glassy state. As shown, at the beginning of the first drying stage (Fig. 8(a)), due to the initial temperature (22 °C) and MC (27% d.b.), all kernel elements were in the rubbery state, located slightly above the glass transition line. After the first drying stage started, the surface layer rapidly lost moisture and transitioned from the rubbery region toward the glassy region at a relatively high rate. After 20 min and 40 min, the glassy region accounted for 14.8% and 19.6% of the whole kernel, respectively. As drying proceeded, the middle layer also exhibited a tendency to shift from the rubbery region toward the glassy region. During tempering (Fig. 8(b)), the glassy area increased by approximately 2.1% within 20 min, from 19.6% to 21.7% of the kernel. Although the glassy fraction increased by the end of tempering, the subsequent second drying stage (Fig. 8(c)) promoted a much faster inward expansion of the glassy region than tempering. Over 60 min, the glassy region expanded by 26.2%. Ultimately, 47.9% of the kernel was located in the glassy region, whereas the central layer remained in the rubbery region.

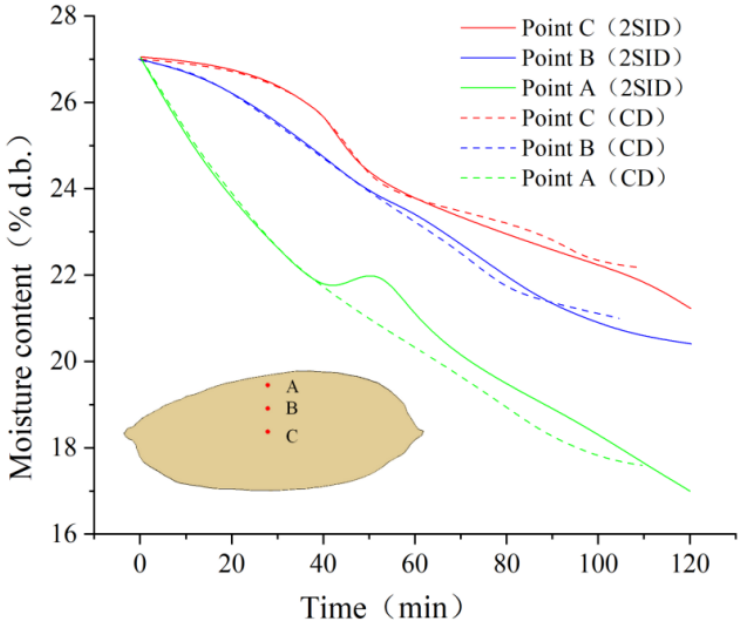

Fig. 7 - Simulated moisture content variations at representative points on the surface (A), in the middle layer (B), and at the center (C) of paddy rice kernels during CD and 2SID

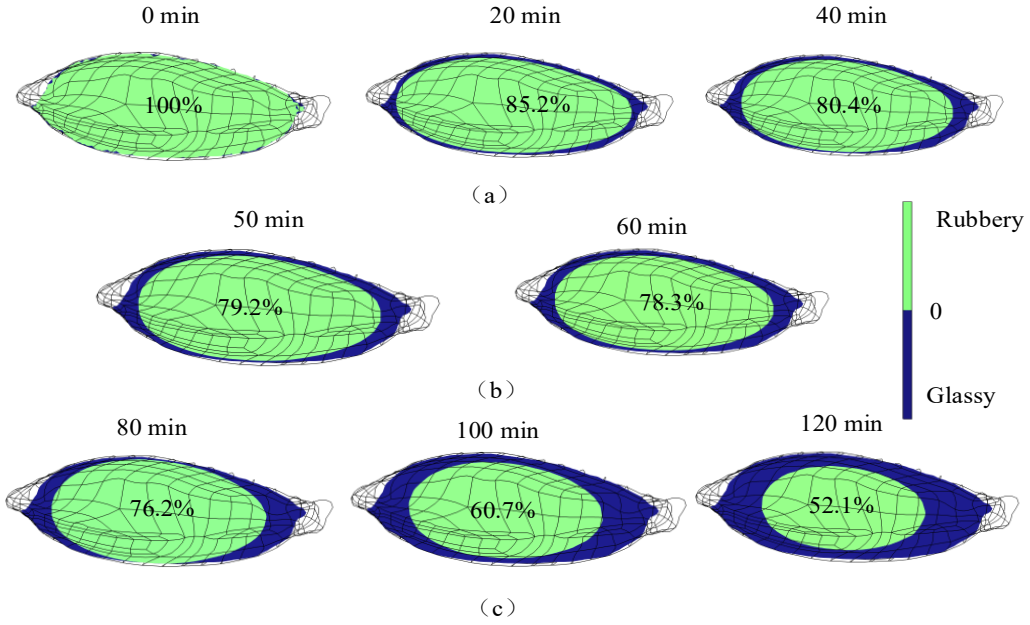

Fig. 8 - Predicted state transition of paddy kernels during 2SID at 45 °C using the developed model: (a) first drying stage; (b) tempering stage; (c) second drying stage

State diagrams at different kernel layers

To investigate layer-dependent behavior during 2SID, the three representative points (A, B, and C) described above were examined. The state evolution at each point was determined by plotting temperature against MC and comparing the trajectory with the glass transition line of the tested cultivar, as shown in Fig. 9.

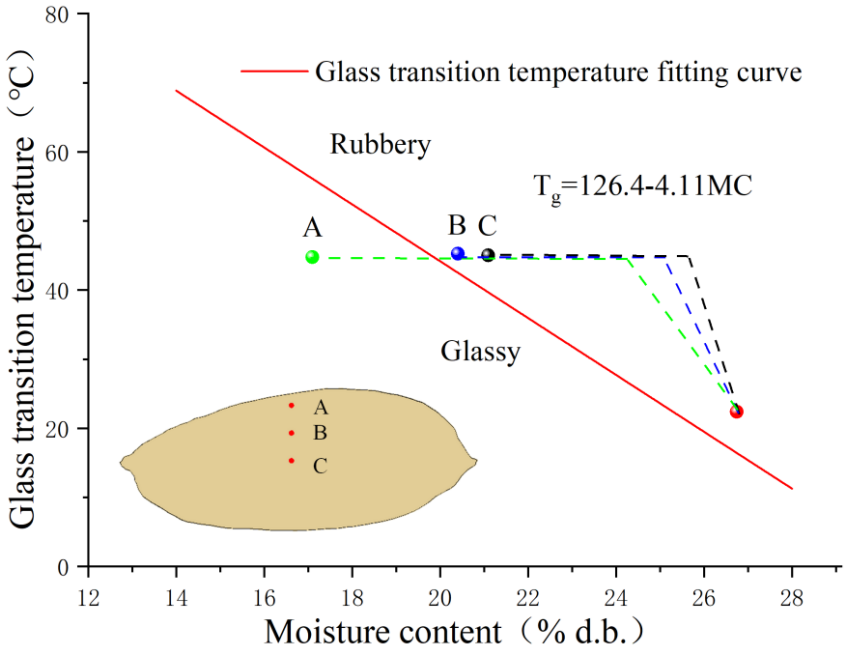

Fig. 9 - State diagrams for representative points on the surface (A), in the middle layer (B), and at the center (C) of paddy kernels during 2SID at 45°C

At the start of the first drying stage, all points were located above the glass transition line. Shortly thereafter, the surface point (A) rapidly lost moisture and exhibited a tendency to approach the glassy state; however, it remained in the rubbery region during the first drying stage. Likewise, points B and C showed slight shifts toward the glassy region, yet they also remained rubbery throughout the first drying stage. After the end of the first drying stage, point A moved slightly back toward the rubbery region, whereas points B and C continued to lose moisture toward the surface. Following tempering, the second drying stage began and the MC at point A decreased progressively. When the MC reached 19.7%, point A underwent glass transition and rapidly entered the glassy region, characterized by a lower diffusion coefficient. Consequently, the distance between the trajectory and the glass transition line increased within the glassy region. Compared with the first drying stage, moisture transfer from points B and C toward the surface occurred at a lower rate. Nevertheless, based on their MC and temperature values, points B and C remained in the rubbery state throughout the entire process.

CONCLUSIONS

Based on the developed and experimentally validated mathematical model, the coupled heat and mass transfer and phase-state evolution of paddy rice during two-stage intermittent drying (2SID) were systematically analyzed and compared with continuous drying (CD).

(1) 2SID improves the internal moisture distribution, alleviates stress concentration, and reduces the likelihood of fissure formation. Model results indicated that, under CD, the moisture gradient between the surface and the core continuously increased as drying progressed. By contrast, at 45 °C, introducing a 20 min tempering step in the 2SID strategy substantially enhanced moisture redistribution from the kernel center toward the outer layers, thereby effectively weakening the residual moisture gradient between the surface and the middle layer at the late drying stage. By mitigating non-uniform hygro-stress induced by moisture differences, 2SID helps reduce structural damage and consequently improves head rice yield.

(2) The tempering stage modulates the glass transition process and is beneficial for quality retention. State identification showed that glass transition initiated at the surface and gradually propagated inward. By the end of the first drying stage, approximately 19.6% of the kernel volume had entered the glassy state.

During tempering, the glassy fraction increased only slightly (by ~2.1%), and its primary contribution was to promote internal moisture redistribution and delay the phase-state transition within the kernel. Ultimately, the glassy fraction reached 47.9%, while the central region remained in the rubbery state throughout the process. This evolution pathway reduces the risk of quality deterioration associated with rapid internal state changes, highlighting the advantage of 2SID in regulating the thermodynamic state of starch.

(3) The proposed model, integrating a realistic 3D geometry and a glass-transition mechanism, is reliable and can serve as an effective tool for optimizing intermittent drying. The model predictions showed strong agreement with the experimental data, with correlation coefficients (R) exceeding 0.95, and accurately captured the dynamic characteristics of the temperature field, moisture field, and state transition. Further analysis indicated that, at 45°C, applying the 2SID strategy not only shortened the overall drying time by 9.09% but also improved drying efficiency and paddy processing quality through the synergistic regulation of moisture gradients and the glass transition process.

Overall, the established model can provide theoretical support and guidance for the design of rice drying equipment, optimization of operating conditions, and development of process control strategies under intermittent drying conditions, and thus shows potential for engineering application and practical implementation.

ACKNOWLEDGEMENT

This work was supported by the Key Research Project on Economic and Social Development of Jiamusi (Grant No. 20250132).

REFERENCES

[1] Arsenoaia, V.-N., Vlăduț, V., Țenu, I., Voicea, I., & Cârlescu, P. M. (2019). Mathematical modeling and numerical simulation of the drying process of seeds in a pilot plant. *INMATEH Agricultural Engineering*, 57(1), 55-62. https://doi.org/10.35633/INMATEH-57-06

[2] Baidhe, E., & Clementson, C. L. (2024). A review of the application of modeling and simulation to drying systems for improved grain and seed quality. *Computers and Electronics in Agriculture, 222, 109094*. https://doi.org/10.1016/j.compag.2024.109094

[3] Cârlescu, P. M., Țenu, I., Roșca, R., Muscalu, A. T., & Vlăduț, N. V. (2018). CFD simulation of an innovative vertical dryer for agricultural seeds drying. Proceedings of the International Symposium on Agricultural Engineering "*Actual Tasks on Agricultural Engineering*", *46*, 419-428.

[4] Chayjan, R. A., Ghasemi, A., & Sadeghi, M. (2018). Stress fissuring and process duration during rough rice convective drying affected by continuous and stepwise changes in air temperature. *Drying Technology, 37*(2), 198-207. https://doi.org/10.1080/07373937.2018.1445637

[5] Delele, M. A., Mihret, Y. C., & Mellmann, J. (2023). Performance evaluation and improvement of prototype rice husk fueled mixed flow rough rice dryer using CFD model. *Drying Technology*, *41*(15), 2447-2463. https://doi.org/10.1080/07373937.2023.2252056

[6] Guo, W., Cheng, S., Cui, Z., He, D., Zhang, X., Shi, T., & Du, J. (2024). Dynamic Drying Characteristics of Alfalfa under Solar Energy-Heat Pump Combined Drying Conditions. *INMATEH Agricultural Engineering*, *73*(2), 569-580. https://doi.org/10.35633/inmateh-73-48

[7] Le, K. H., Tran, T. T. H., Kharaghani, A., & Tsotsas, E. (2019). Experimental benchmarking of diffusion and reduced models for convective drying of single rice grains. *Drying Technology*, 38(*2*), 200-210. https://doi.org/10.1080/07373937.2019.1648288

[8] Liu, W., Chen, G., Zheng, D., Ge, M., & Liu, C. (2023). Effects of the Broken Kernel on Heat and Moisture Transfer in Fixed-Bed Corn Drying Using Particle-Resolved CFD Model. *Agriculture, 13*(8), .1470. https://doi.org/10.3390/agriculture13081470

[9] Liu, W., Chen, G., Zheng, D., Ge, M., & Liu, C. (2023). Numerical and experimental investigation of flow and heat transfer in a fixed bed of non-spherical grains using the DEM-CFD method. *Journal of Food Process Engineering, 46*(8), 14362. https://doi.org/10.1111/jfpe.14362

[10] Liu, Z., Che, G., Wan, L., Wang, H., Chen, Z., & Wang, H. (2024). Design and Experimental Verification of Self-Priming Hot Air Temperature Changing Device for Grain Dryer. *INMATEH Agricultural Engineering*, *73*(2)*,* 310-323. https://doi.org/10.35633/inmateh-73-26

[11] Mahmood, N., Liu, Y., Zheng, X., Munir, Z., Pandiselvam, R., Zhang, Y., & Lei, D. (2024). Influences of emerging drying technologies on rice quality. *Food Research International, 184*, 114264. https://doi.org/10.1016/j.foodres.2024.114264

[12] Nasrnia, E., Sadeghi, M., Raeisi Isa-Abadi, A., & Mireei, S. A. (2024). A novel simulation model to analyze rice intermittent drying considering glass transition concept. *Journal of Food Engineering, 364*, 111819. https://doi.org/10.1016/j.jfoodeng.2023.111819

[13] Srisang, N., Soponronnarit, S., Thuwapanichayanan, R., & Prachayawarakorn, S. (2015). Modeling heat and mass transfer–induced stresses in germinated brown rice kernels during fluidized bed drying. *Drying Technology*, *34*(6), 619-634. https://doi.org/10.1080/07373937.2015.1066385

[14] Wang, C., Pei, Y., Mu, Z., Fan, L., Kong, J., Tian, G., & Qiu, H. (2024). Simulation Analysis of 3-D Airflow and Temperature Uniformity of Paddy in a Laboratory Drying Oven. *Foods, 13*(21), 3466. https://doi.org/10.3390/foods13213466

[15] Wang, H., Che, G., Wan, L., Chen, Z., Sun, W., & Tang, H. (2023). Effect of variable temperature levels on drying characteristics and quality indices of rice in continuous drying and multi-stage intermittent drying. *Journal of Food Process Engineering, 46*(7), 14356. https://doi.org/10.1111/jfpe.14356

[16] Wang, H., Che, G., Wan, L., & Tang, H. (2022). Effects of drying approaches combined with variable temperature and tempering on the physicochemical quality of rice. *Drying Technology, 41*(7), 1199-1213. https://doi.org/10.1080/07373937.2022.2133140

[17] Wang, H., Wang, Z., Che, G., Wan, L., & Chen, Z. (2025). Research on the Prediction Model and Formation Law of Drying Cracks of Paddy Based on Multi-Physical Field Coupling. *Agriculture, 15*(4), 383. https://doi.org/10.3390/agriculture15040383

[18] Ying, T., & Spang, E. S. (2024). Paddy Drying Technologies: A Review of Existing Literature on Energy Consumption. *Processes, 12*(3), 532. https://doi.org/10.3390/pr12030532

[19] Zhang, L., Jiang, L., Adnouni, M., Li, S., & Zhang, X. (2024). Numerical Study on the Variable-Temperature Drying and Rehydration of Shiitake. *Foods, 13*(21), 3356. https://doi.org/10.3390/foods13213356

[20] Zhao, L., Yang, J., Wang, S., & Wu, Z. (2019). Investigation of glass transition behavior in a rice kernel drying process by mathematical modeling. Drying Technology, *38*(8), 1092-1105. https://doi.org/10.1080/07373937.2019.1612427